Regulating phase separation and molecular stacking by introducing siloxane to small-molecule donors enables high efficiency all-small-molecule organic solar cells

Yilin Chang,[‡ab] Xiangwei Zhu,[‡c] Yanan Shi,[ab] Yanan Liu,[a] Ke Meng,[ab] Yanxun Li,[ab] Jingwei Xue[d] Lingyun Zhu,[a] Jianqi Zhang,[a] Huiqiong Zhou,[ab] Wei Ma,[d] Zhixiang Wei,[ab] and Kun Lu,[ab]*

[a] CAS Key Laboratory of Nanosystem and Hierarchical Fabrication, CAS Center for Excellence in Nanoscience, National Center for Nanoscience and Technology, Beijing 100190, PR China.

[b] University of Chinese Academy of Sciences, Beijing 100049, PR China.

[c] College of Textiles & Clothing, State Key Laboratory of Bio-Fibers and Eco-Textiles, Qingdao University, Qingdao, 266071 China

[d] State Key Laboratory for Mechanical Behavior of Materials, Xi'an Jiaotong University, Xi'an 710049, PR China.

* Email: lvk@nanoctr.cn

Materials

Solvents and other common reagents were obtained from Beijing Chemical Plant. All other chemicals were purchased from commercial sources (Alfa, Acros, TCI, J&K, and Sigma–Aldrich) and used without further purification unless otherwise stated. Compound 1, 2 was purchased from Suna Tech Inc. Compound 4 was purchased from Hyper Inc. Y6 was purchased from Solarmer Materials Inc. The synthetic details are as follows.

The synthesis procedures of three small-molecule donors involve two key steps: one is the synthesis of the central DTBDT unit with trimethyltin groups, and the other is the synthesis of a composite of π bridge (bithiophene) and end group (rhodanine). As the synthesis of each type of intermediate can be carried out independently, the target small-molecules have been effectively obtained only by one step Stille-coupling reaction.
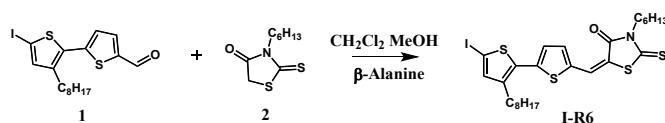
Scheme S1

I-R6: compound 1 (700 mg, 1.6 mmol), compound 2 (1100 mg, 4.9 mmol), and β-alanine (14 mg, 0.16 mmol) were dissolved in a mixture of dichloromethane (20 ml) and methanol (10 ml) in a three-neck flask. After stirring at 60 °C overnight, the reaction mixture was poured into water and extracted several times with dichloromethane. Then the solvent was removed under reduced pressure, and the crude product was purified

by column chromatography on silica gel to yield I-R6 as red solid (570 mg, 56% yield).

MALDI-TOF MS (m/z): 631.71. ^{1}H NMR (400 MHz, CDCl$_3$): δ (ppm) 7.85 (s, 1H), 7.37-7.36 (d, 1H), 7.16-7.15 (d, 1H), 6.96 (s, 1H), 4.15-4.11 (m, 2H), 2.79-2.75 (m, 2H), 1.75-1.64 (m, 4H), 1.41-1.30 (m, 16H), 0.93-0.88 (m, 6H).
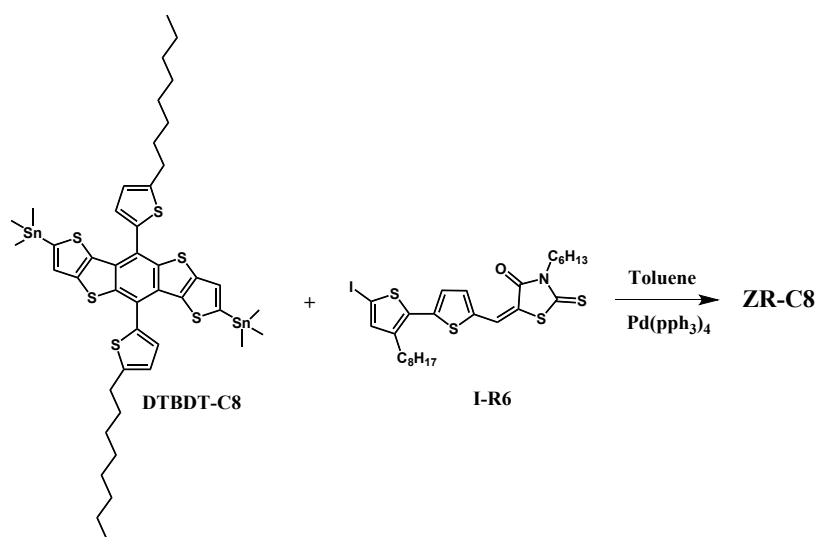
Scheme S2

ZR-C8: compound DTBDT-C8 (200 mg, 0.2 mmol), compound I-R6 (380 mg, 0.6 mmol) and Pd(PPh$_3$)$_4$ (35 mg, 0.03 mmol) were dissolved into toluene (30 ml) in a three-neck flask. Then the flask was subjected to three successive cycles of vacuum followed by refilling with argon. After stirring at 110 ^{o}C overnight, the reaction mixture was poured into water and extracted several times with chloroform. Then the solvent was removed under reduced pressure, and the crude product was purified by column chromatography on silica gel to yield ZR-C8 as aubergine solid (230 mg, 70% yield).

MALDI-TOF MS (m/z): 1698.0. ^{1}H NMR (400 MHz, CDCl$_3$): δ (ppm) 7.72 (s, 2H), 7.26-7.24 (m, 4H), 7.19 (d, 2H), 7.09-7.07 (m, 4H), 6.85 (s, 2H), 4.02-3.99 (t, 4H), 3.08-3.04 (t, 4H), 2.73-2.70 (t, 4H), 1.93-1.86 (m, 4H), 1.65-1.54 (m, 16H), 1.45-1.26 (m, 44H), 0.92-0.85 (m, 18H). ^{13}C NMR (100 MHz, CDCl$_3$): δ (ppm) 191.84, 167.18,

148.43, 143.86, 143.14, 142.05, 139.53, 136.61, 136.27, 134.18, 134.15, 133.97, 133.93, 132.37, 129.62, 129.04, 128.65, 126.85, 126.10, 124.68, 122.94, 119.77, 116.08, 44.71, 31.99, 31.97, 31.84, 31.29, 30.46, 30.16, 29.87, 29.59, 29.45, 29.41, 29.21, 26.86, 26.45, 22.79, 22.77, 22.53, 14.20, 14.01. Anal. Calcd. For $C_{90}H_{108}N_2O_2S_{14}$: C, 63.64; H, 6.41; N, 1.65; S, 26.42. Found: C, 63.79; H, 6.40; N, 1.87; S, 26.39.
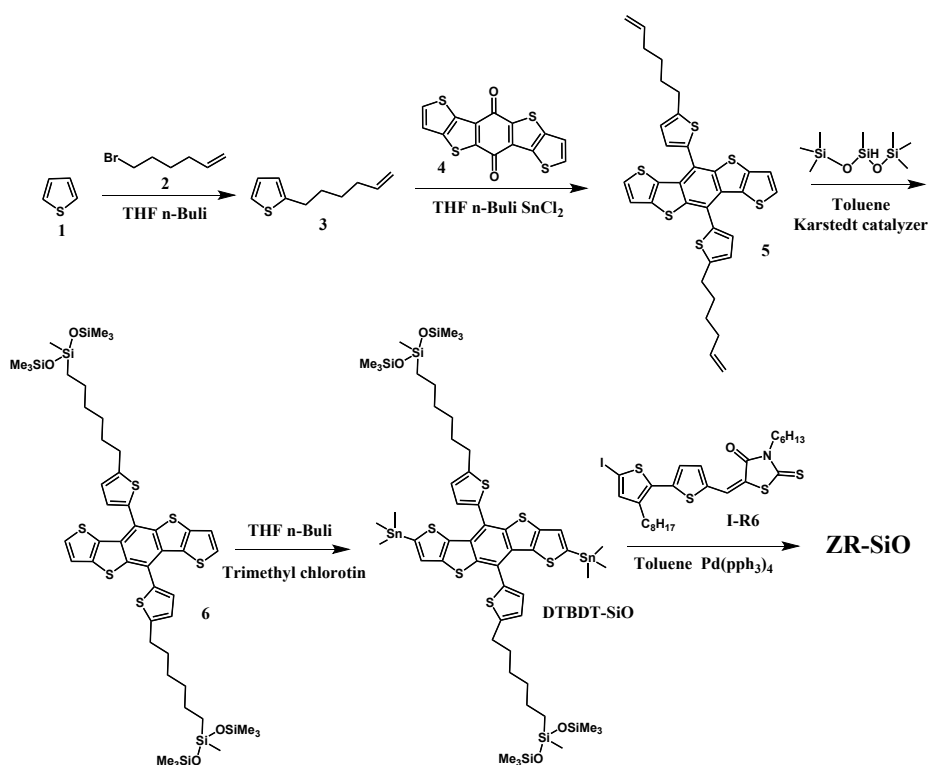
Scheme S3

ZR-SiO: The synthesis of small molecule mainly consists of five steps.

(1) The synthesis of Compound 3: Compound 1 (2 g, 23.8 mmol) was dissolved in 20ml tetrahydrofuran solvent in a three-neck flask, and the reaction temperature was lowered to -78 °C. Then n-Buli (18 ml) was slowly added to the mixture by drop, and the reaction mixture was kept at -78 °C for 1 hour. After the reaction mixture temperature was raised to -20 ° C, compound 2 (4.5 g, 28 mmol) was added

and reacted overnight at room temperature. The reaction mixture was poured into water and extracted several times with dichloromethane. Then the solvent was removed under reduced pressure, and the crude product was purified by vacuum distillation. The pure compound 3 (3.2 g, 82% yield) was obtained as a clear oily liquid. MALDI-TOF MS (m/z): 166. ^{1}H NMR (400 MHz, CDCl$_3$): δ (ppm) 7.12-7.11 (dd, 1H), 6.93-6.91 (q, 1H), 6.79-6.78 (m, 1H), 5.87-5.77 (m, 1H), 5.05-4.94 (m, 2H), 2.86-2.82 (m, 2H), 2.13-2.07 (m, 2H), 1.75-1.67 (m, 2H), 1.52-1.44 (m, 2H).

(2) The synthesis of Compound 5: Compound 3 (2 g, 12 mmol) was dissolved in 20ml tetrahydrofuran solvent in a three-neck flask, and the reaction temperature was lowered to -5 °C. Then n-Buli (8 ml) was slowly added to the mixture by drop, and the reaction mixture was reacted at room temperature for 30 min. In order to ensure the solubility, excess tetrahydrofuran was added into the reaction solution, and the reaction temperature was raised to 90 °C after compound 4 (1.3 g, 4 mmol) was added. After stirring at 90 °C overnight, the reaction mixture was stirred with stannous chloride (SnCl$_2$) (6 g, 32 mmol) solution dissolved in dilute hydrochloric acid (16 ml), and the reaction mixture was poured into water and extracted several times with dichloromethane. Then the solvent was removed under reduced pressure, and the crude product was purified by column chromatography on silica gel to yield compound 5 (1 g, 40% yield). MALDI-TOF MS (m/z): 630. ^{1}H NMR (400 MHz, CDCl$_3$): δ (ppm) 7.40-7.38 (d, 2H), 7.24-7.23 (d, 2H), 7.17 (d, 2H), 7.01-7.00 (d, 2H), 5.92-5.81 (m, 2H), 5.09-5.03 (m, 2H), 5.00-4.97 (m, 2H), 3.02-2.98 (t, 4H),

2.19-2.14 (m, 4H), 1.88-1.81 (m, 4H), 1.63-1.55 (m, 4H).

(3) The synthesis of Compound 6: Compound 5 (1 g, 1.6 mmol), 1,1,1,3,5,5,5-heptamethyltrisiloxane (890 mg, 4 mmol) and Karstedt Catalyst (220 mg, 0.4 mmol) were dissolved in 20ml toluene in a three-neck flask. Then the flask was subjected to three successive cycles of vacuum followed by refilling with argon. After stirring at 75 °C overnight, the reaction mixture was poured into water and extracted several times with dichloromethane. Then the solvent was removed under reduced pressure, and the crude product was purified by column chromatography on silica gel to yield compound 6 (1.5 g, 90% yield). MALDI-TOF MS (m/z): 1076. ^{1}H NMR (400 MHz, CDCl$_3$): δ (ppm) 7.40-7.39 (d, 2H), 7.24-7.23 (d, 2H), 7.18-7.17 (d, 2H), 7.01-7.00 (d, 2H), 3.01-2.97 (t, 4H), 1.86-1.78 (m, 4H), 1.49-1.37 (m, 12H), 0.52-0.48 (m, 4H), 0.10-0.09 (m, 36H), 0.03-0.02 (m, 6H).

(4) The synthesis of DTBDT-SiO: Compound 6 (1.5 g, 1.4 mmol) was dissolved in 20ml tetrahydrofuran solvent in a three-neck flask, and the reaction temperature was lowered to -78 °C. Then n-Buli (4 ml) was slowly added to the mixture by drop and the reaction mixture was kept at -78 °C for 2 hours. After the addition of trimethyltin chloride (11 ml), the reaction mixture was stirred at -78 °C for 1 hour. After stirring at room temperature overnight, the reaction mixture was poured into water and extracted several times with dichloromethane. Then the solvent was removed under reduced pressure, and the crude product did not need purification. MALDI-TOF MS (m/z): 1400.

(5) The synthesis of ZR-SiO: The crude product DTBDT-SiO, which obtained in the

fourth step, is directly dissolved in 30 ml toluene with compound I-R6 (2.6 g, 4.2 mmol) and Pd(PPh$_3$)$_4$ (200 mg, 0.2mmol) in a three-neck flask. Subsequent reaction details and purification are similar to ZR-C8. MALDI-TOF MS (m/z): 2082.5. ^{1}H NMR (400 MHz, CDCl$_3$): δ (ppm) 7.79 (s, 2H), 7.31-7.30 (d, 2H), 7.23 (d, 2H), 7.21 (s, 2H), 7.15-7.14 (d, 2H), 7.09 (d, 2H), 6.94 (s, 2H), 4.09-4.05 (t, 4H), 3.10-3.06 (t, 4H), 2.79-2.76 (t, 4H), 1.93-1.89 (t, 4H), 1.73-1.66 (m, 10H), 1.57-1.28 (m, 40H), 0.92-0.86 (m, 20H), 0.55-0.51 (m, 4H), 0.12 (m, 36H). ^{13}C NMR (100 MHz, CDCl$_3$): δ (ppm) 191.90, 167.27, 148.57, 143.92, 143.19, 142.15, 139.71, 139.62, 136.76, 136.41, 134.26, 133.90, 132.47, 129.72, 129.16, 128.68, 127.02, 126.22, 124.69, 124.65, 123.14, 119.91, 116.18, 44.75, 33.03, 31.95, 31.82, 31.31, 30.53, 30.20, 30.12, 29.81, 29.56, 29.41, 29.08, 26.88, 26.45, 23.14, 22.77, 22.53, 17.71, 14.20, 14.01, 1.93. Anal. Calcd. For C$_{100}$H$_{140}$N$_2$O$_6$S$_{14}$Si$_6$: C, 57.65; H, 6.77; N, 1.34; S, 21.54. Found: C, 57.74; H, 6.77; N, 1.59; S, 21.66.
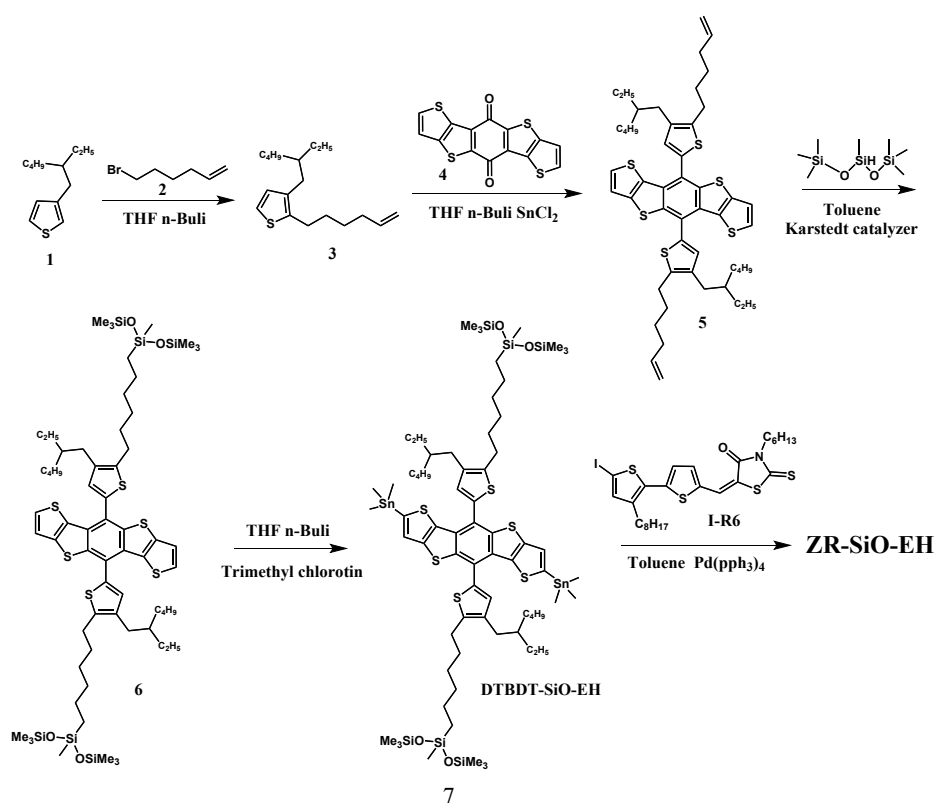
Scheme S4

ZR-SiO-EH: Except for the difference of raw materials (compound 1), the synthesis method of small molecules is basically the same as that of ZR-SiO. The detailed synthesis route is not repeated here, but the molecular information of products in each step is listed.

(1) Compound 3 for Scheme S4: MALDI-TOF MS (m/z): 278.5. ^{1}H NMR (400 MHz, CDCl$_3$): δ (ppm) 7.03-7.01 (d, 1H), 6.78-6.77 (d,1H), 5.87-5.76 (m, 1H), 5.04-4.94 (m, 2H), 2.74-2.71 (t, 2H), 2.44-2.42 (d, 2H), 2.12-2.07 (q, 2H), 1.70-1.62 (m, 3H), 1.28-1.25 (m, 10H), 0.9-0.85 (m, 6H).

(2) Compound 5 for Scheme S4: MALDI-TOF MS (m/z): 855.4. ^{1}H NMR (400 MHz, CDCl$_3$): δ (ppm) 7.38-7.37 (d, 2H), 7.24-7.23 (d, 2H), 7.03 (s, 2H), 5.91-5.81 (m, 2H), 5.08- 4.96 (m, 4H), 2.91-2.88 (t, 4H), 2.58-2.57 (d, 4H), 2.18-2.13 (m, 4H), 1.83-1.76 (m, 4H), 1.65-1.57 (m, 24H), 0.95-0.86 (m, 12H).

(3) Compound 6 for Scheme S4: MALDI-TOF MS (m/z): 1300.4. ^{1}H NMR (400 MHz, CDCl$_3$): δ (ppm) 7.39-7.37 (d, 2H), 7.24-7.23 (d, 2H), 7.05 (s, 2H), 2.92-2.88 (t, 4H), 2.60-2.59 (d, 4H), 1.70-1.64 (m, 10H), 1.44-1.28 (m, 24H), 0.99-0.80 (m, 22H), 0.11-0.09 (m, 36H)

(4) ZR-SiO-EH: MALDI-TOF MS (m/z): 2305.6. ^{1}H NMR (400 MHz, CDCl$_3$): δ (ppm) 7.79 (s, 2H), 7.30 (s, 2H), 7.27 (s, 2H), 7.15 (s, 2H), 7.05 (s, 2H), 6.95 (s, 2H), 4.08-4.05 (t, 4H), 2.95-2.92 (t, 4H), 2.78-2.76 (t, 4H), 2.63-2.62 (t, 4H), 1.83-1.81 (m, 4H), 1.68 (m, 10H), 1.43-1.32 (m, 66H), 0.99-0.89 (m, 24H), 0.52-0.49 (m, 4H), 0.24-0.09 (m, 36H). ^{13}C NMR (100 MHz, CDCl$_3$): δ (ppm) 192.06, 167.46,

144.06, 143.18, 142.39, 140.10, 140.05, 139.85, 137.73, 137.47, 137.10, 136.88, 134.50, 131.88, 130.93, 129.92, 129.23, 127.29, 126.60, 124.84, 123.73, 120.30, 116.53, 44.85, 40.70, 33.11, 32.74, 32.60, 32.03, 31.91, 31.34, 30.38, 30.00, 29.72, 29.51, 29.33, 29.01, 28.96, 28.43, 26.93, 26.39, 25.72, 23.25, 23.15, 22.72, 22.52, 17.68, 14.24, 14.15, 14.01, 11.05, 1.90. Anal. Calcd. For $C_{116}H_{172}N_2O_6S_{14}Si_6$: C, 60.37; H, 7.51; N, 1.21; S, 19.45. Found: C, 60.40; H, 7.52; N, 1.24; S, 19.39.

Measurements and characterizations

Molecular characterization

Mass spectra were determined on a Bruker microflex MALDI-TOF mass spectrometer. ^{1}H NMR was obtained on a Bruker Avance 400 NMR spectrometer using tetramethylsilane as an internal standard. UV-vis absorption spectra were recorded on a Shimadzu UV-3600 UV-VIS-NIR spectrophotometer. Electrochemical cyclic voltammetry was conducted on a CHI 760E workstation with Pt plate coated with the small molecule film, Pt plate, and Ag/Ag^+ electrode as the working electrode, counter electrode, and reference electrode, respectively, in a 0.1 mol/L tetrabutylammonium hexafluorophosphate (Bu4NPF6) acetonitrile solution. Ag/Ag^+ electrode potentials were calibrated with the ferrocene/ferrocenium (Fc/Fc^+) redox couple (-4.8 eV relative to the vacuum level). Contact angle (θ) in solutions of ZR-type donors and Y6 are measured on ITO/glass substrate by using the pendant drop method with the XG-CAMB3 standard contact angle meter.

The calculation of surface tension by DCA (dynamic contact angle)

Contact angles were measured with a contact angle meter (GBX DIGIDROP). The solution of each organic material was spin-coated on cleaned ITO substrates. Droplets of water and diiodomethane were dripped onto the different films.

According to Owens-Wendt method, surface energy could be divided into dispersive and polar components.

$$\gamma = \gamma^d + \gamma^p \quad (1)$$

Furthermore, the dispersive and polar surface energy can be calculated though the formula below based on the contact angles obtained by two solvents.

$$(1 + \cos\theta)\gamma_l = \frac{4\gamma_l^d\gamma_s^d}{\gamma_l^d + \gamma_s^d} + \frac{4\gamma_l^P\gamma_s^P}{\gamma_l^P + \gamma_s^P} \quad (2)$$

where θ is the contact angle of a specific solvent, γ_L is the surface energy of the solvent, γ_S^d and γ_S^P refer to the dispersive and polar surface energy of the solid, respectively, and γ_L^d and γ_L^P refer to the dispersive and polar surface energy of the solvent, respectively.

Thus, the unknown value γ_S^d and γ_S^P can be solved though combining two equations obtained by contact angle measurement of two different solvents.

Solubility parameter (δ) can be calculated from the surface energy,

$$\delta = K\sqrt{\gamma} \quad (3)$$

where γ is the surface energy, K is the proportionality constant ($K = 116 \times 10^3 \, \text{m}^{-1/2}$).

And Flory–Huggins interaction parameter (χ_{ij}) can be written as a function of two solubility parameter,

$$\chi_{ij} = \frac{V_0}{RT}(\delta_i - \delta_j) \quad (4)$$

where χ_{ij} is the Flory–Huggins interaction parameter between the material i and j, V_0 is

the geometric mean of the molecular molar volume, R is the gas constant, T is the absolute temperature, and δ_i and δ_j are the solubility parameter of material i and j, respectively.

To simplify, we define the parameter $\kappa = K^2 V_0 / RT$, then the Flory–Huggins interaction parameter can be written as the formula below,

$$\chi_{ij} = \kappa(\sqrt{\gamma_i} - \sqrt{\gamma_j})^2 \quad (5)$$

where γ_i and γ_j are the surface energy of material i and j, respectively.

Differential scanning calorimetry

Differential scanning calorimetry (DSC) was performed on TA DSC Q2000 differential scanning calorimeter with a heating/cooling rate of 20 °C min^{-1} from 0 °C to 300 °C for two heating/cooling circles. The data of the first circle was presented. The Flory–Huggins interaction parameter (χ) was calculated from the Nishi-Wang equation:

$$\frac{1}{T_m} - \frac{1}{T_m^0} = -\frac{R}{\Delta H_m} \frac{V_2}{V_1} \left[\frac{\ln \varnothing_2}{m_2} + \left(\frac{1}{m_2} - \frac{1}{m_1} \right) \times (1 - \varnothing_2) + \chi(1 - \varnothing_2)^2 \right] \quad (6)$$

Where substance 1 & 2 are two components in the blend, T_m is the melting temperature of the mixture, and T_m^0 is the melting temperature of substance 2, R is the gas constant, ΔH_m is the melting enthalpy of substance 2, V is the monomer molar volume, $\varnothing$ is the volume fraction, and m is the degree of polymerization. Considering that substance 1 & 2 are small molecules, the value of m_1 and m_2 can be approximately equal to 1.

Fabrication and Characterization of Organic Solar Cells

All-small-molecule devices were fabricated with conventional device structure of

ITO/PEDOT:PSS/active layer/PNDIT-F3N/Ag. The PEDOT:PSS solution was spin-coated on top of the cleaned ITO-coated glass substrate and the PEDOT:PSS film thickness was approximately 30 nm. After annealing at 150 °C for 20 min, then the substrates were transferred into a glove box. The mixture of small donors and Y6 with total concentration ca. 16-18 mg ml^{-1} stirred at 50 °C in chloroform for ca. 1.5 h until they intensively dissolved. Among them, the solubility of ZR-SiO is relatively low, and its total concentration is 16 mg ml^{-1}. A very small amount of chloronaphthalene (CN) is added as an additive to the preparation of the solution, at 0.2% of the volume fraction of the total solution. Subsequently, the active layer was spin-coated from blend chloroform solutions with a rotation speed in the range of 1400-2000 r/min. After thermal annealing at 120 °C for 10 min, a concentration of 0.2 mg/ml PNDIT-F3N with a small amount of acetic acid spin-coated on the active layer with a rotation speed of 2000 r/min. Finally, a layer of ∼100 nm Ag layer was evaporated under a high vacuum ($<1 \times 10^{-4}$ Pa).

The J–V curves were obtained by a Keithley 2400 source measure unit. Device J–V characteristics was measured under AM 1.5 G (100 mW cm^{-2}) using a Newport Thermal Oriel 91159A solar simulator. Light intensity is calibrated with a Newport Oriel PN 91150V Si-based solar cell. The effective area of the device is 0.04 cm^2. The EQE measurements of the devices were performed in air with an Oriel Newport system (Model 66902) equipped with a standard Si diode. Monochromatic light was generated from a Newport 300 W lamp source. The thickness of the active layer was measured on a Kla-TencorAlpha-StepD-120 Stylus Profiler. Transient photovoltage (TPV) was

measured by applying a 488 nm solid-state laser (Coherent OBIS CORE 488LS) with a pulse width of ~30 ns. Under open-circuit conditions, photovoltage traces were registered by the oscilloscope with an external 10 MΩ resistor in series.

Energy Loss

Highly sensitive EQE was measured using an integrated system (PECT-600, Enlitech), where the photocurrent was amplified and modulated by a lock-in instrument. EQEEL measurements were performed by applying external voltage/current sources through the devices (ELCT-3010, Enlitech). EQEEL measurements were performed for all devices according to the optimal device preparation conditions.

The E_{loss} in organic solar cells can be divided into three parts as follows:

$$E_{loss} = E_g^{pv} - qV_{OC}$$

$$= \left(E_g^{pv} - qV_{OC}^{SQ}\right) + \left(qV_{OC}^{SQ} - qV_{OC}^{rad}\right) + \left(qV_{OC}^{rad} - qV_{OC}\right)$$

$$= \left(E_g^{pv} - qV_{OC}^{SQ}\right) + q\Delta V_{OC}^{rad,\ below\ gap} + q\Delta V_{OC}^{non-rad}$$

$$= q\Delta V_1 + q\Delta V_2 + q\Delta V_3$$

$$= \Delta E_1 + \Delta E_2 + \Delta E_3 \qquad\qquad (7)$$

$$E_g^{pv} = \frac{\int_a^b E_g.P(E_g).dE_g}{\int_a^b P(E_g).dE_g} \qquad\qquad (8)$$

In this formula, q is the elementary charge; V_{OC}^{SQ} is the maximum voltage in the Shockley–Queisser (SQ) limit model, and V_{OC}^{rad} is the open-circuit voltage with only radiative recombination in the device. The integral boundaries a and b are selected

where P(a) = P(b) = 0.5max $P(E_g)$. The selection of integral boundaries serves to exclude the influence of noisy data and negative value of $P(E_g)$, and is not physically motivated. While the factor 0.5 in the choice of a and b is pretty arbitrary, slightly different choices would not strongly affect the result except for very noisy data.

Hole-only and electron-only devices fabrication and measurement

The charge carrier mobilities of polymers and blend films were measured by the space-charge limited current (SCLC) method with device structures of ITO/PEDOT:PSS/active layer/Au for hole-only devices and Al/active layer/Al for electron-only devices. The blend films were prepared under the optimal conditions for solar cell devices.

J–V characteristics were measured in the range of 0-5 V using a Keithley 2400 source-measure unit in the dark. For the fitting, an SCLC model was used mathematically expressed as:

$$J = \frac{9}{8}\varepsilon_0\varepsilon_\gamma\mu_0\frac{(V - V_{bi})^2}{L^3}exp(0.89\gamma\sqrt{\frac{V - V_{bi}}{L}})J = \frac{9}{8}\varepsilon_0\varepsilon_r\mu_0\frac{(V - V_{bi})^2}{L^3}exp\left(0.89\gamma\sqrt{\frac{V - V_{bi}}{L}}\right) \quad (9)$$

Where ε_0, ε_r is the dielectric constant of the semiconductor layer, μ_0 is the zero-field mobility, V_{bi} is the built-in potential due to the anode-cathode work function offset, L is the thickness of the active layer, and γ is the field-dependence coefficient. The exponential term in Eq. S9 describes the field-dependence of the diode mobility.

TEM, AFM, GIWAXS and XPS

Transmission electron microscopy (TEM) measurements were performed on a Tecnai G2 F20 U-TWIN instrument under proper defocus conditions. The atomic force

14

microscopy (AFM) measurements were performed on Bruker Multimode 8HR. Grazing incidence wide-angle x-ray scattering (GIWAXS) experiments were conducted at the beamline of 7.3.3 at the Advanced Light Source (ALS). Samples were prepared on Si/PEDOT: PSS substrates. X-ray photoelectron spectroscopy (XPS) samples were prepared on a glass substrate without the top electrode (glass/PEDOT:PSS/target films)

AFM-IR

The atomic force microscopy-infrared spectroscopy (AFM-IR) measurements were performed on NanoIR2-fs. AFM-IR is a photothermal technique that combines AFM and IR spectroscopy to unambiguously identify the chemical composition of a sample with tens-of-nanometers spatial resolution. When the sample absorbs photons from a pulsed tunable monochromatic IR laser light source, it heats up and rapidly expands, inducing an impulse to the AFM probe in contact with the sample. This causes an oscillation of the AFM cantilever at its contact resonant frequencies. The tip is then scanned across the sample surface, and the topography of the sample is recorded.

As to the systems we studied, because of the very similar structure of the three small molecule donors, they all showed obvious infrared absorption peaks at 1580 cm^{-1} (Figure S13). However, the small molecule acceptor (Y6) basically shows no infrared absorption at this characteristic wavelength (Figure S13). Therefore, the IR laser light with a fixed wavenumber of 1580 cm^{-1} was focused onto the sample, and high-resolution AFM-IR image can be acquired by scanning the AFM probe across the surface of the blend film, composed of the small molecule donor and Y6. When the AFM tip intermittently contacts a small molecule donor domain, a strong resonant

response appears. When the AFM tip moves to a Y6 domain location, the signal gets much weaker. So, for the AFM-IR image, the warm color region (yellow and red) with strong signals can be considered as the small molecule donor enriched domain, while the cold color region (blue) with weak signals can be regarded as the small molecule acceptor enriched domain (Figure 4d-f). And then, the obvious phase separation between donor and acceptor for the blend film can be easily obtained according to the AFM-IR image.

RSoXS characterization

R-SoXS measurements were performed at the beamlines 7.3.3 and 11.0.1.2, ALS,Lawrence Berkeley National Laboratory. The samples were prepared in a similar manner as for TEM and transferred to a 1.5 mm × 1.5 mm, 100 nm thick Si3N4 membrane supported by a 5 mm × 5 mm, 200 μm thick Si frame (Norcada Inc.). 2D scattering patterns were collected on an in-vacuum charge-coupled device camera (Princeton Instrument PI-MTE). The sample detector distance was calibrated from diffraction peaks of a triblock copolymer poly(isoprene-b-styrene-b-2-vinyl pyridine), which presents a known spacing of 391 Å. The beam size at the sample is ≈100 μm by 200 μm.

Supplementary Figures
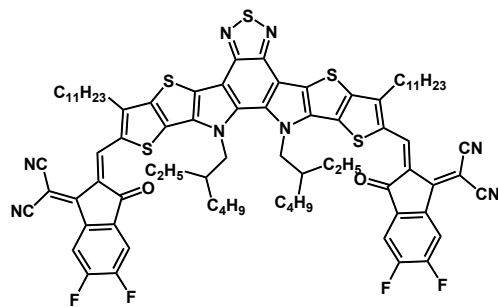
Figure S1 The chemical structures of Y6.
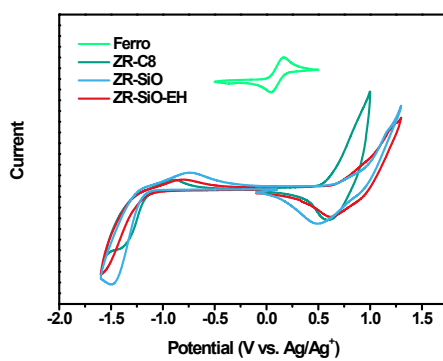
Figure S2 Electrochemical cyclic voltammetry curves of these donor films measured in 0.1 mol L^{-1} Bu$_4$NPF$_6$ acetonitrile solutions.
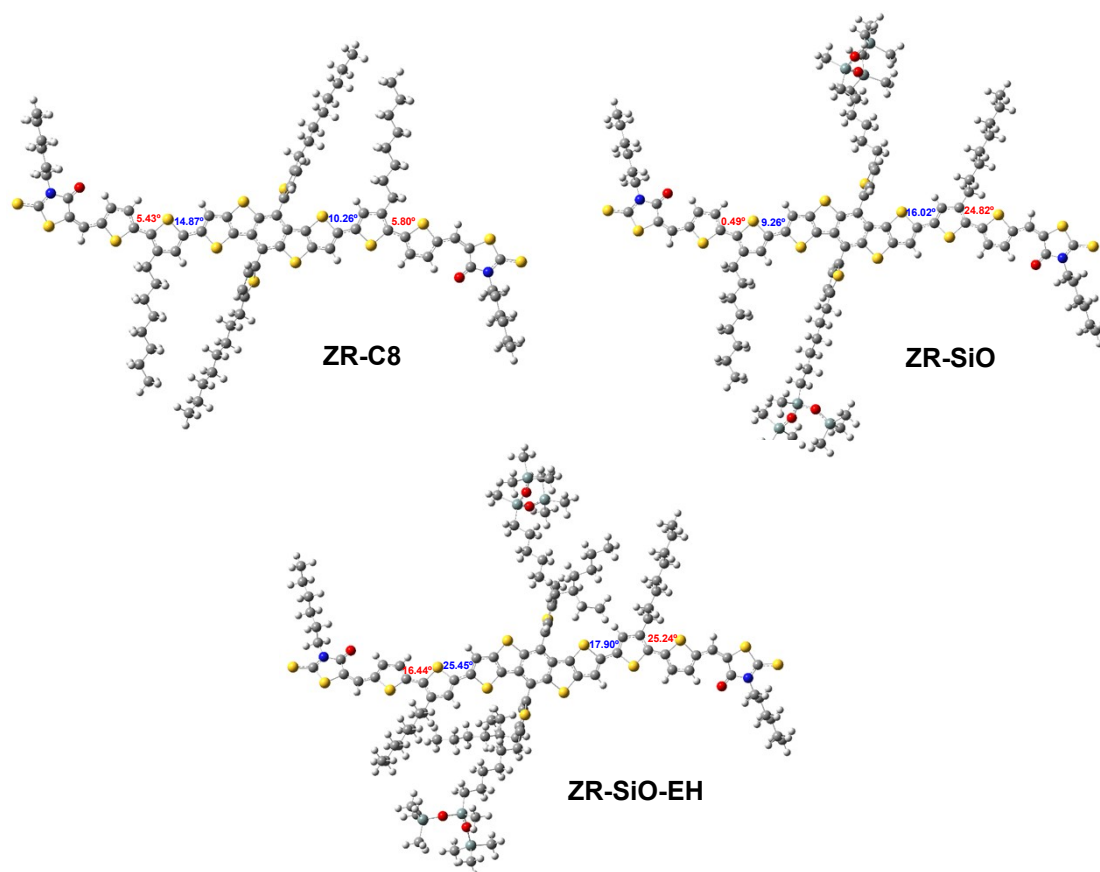
Figure S3 The optimized molecular geometries for ZR-C8, ZR-SiO and ZR-SiO-EH with the whole alkyl chains according to the density functional theory (DFT) calculations, performed at the B3LYP/6-31G (d, p) level.
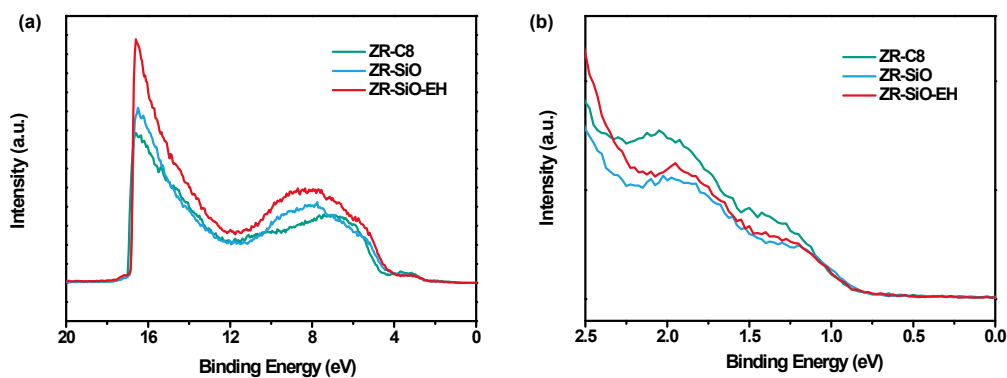
Figure S4 (a) Ultraviolet photoelectron spectroscopy (UPS) of ZR-C8, ZR-SiO and ZR-SiO-EH in thin films. (b) the local enlarged drawing near Fermi edge.
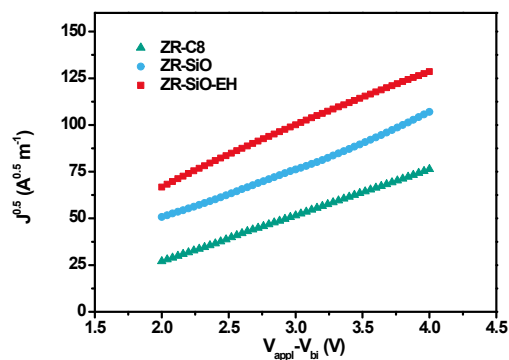
Figure S5 Hole mobility of donor films.
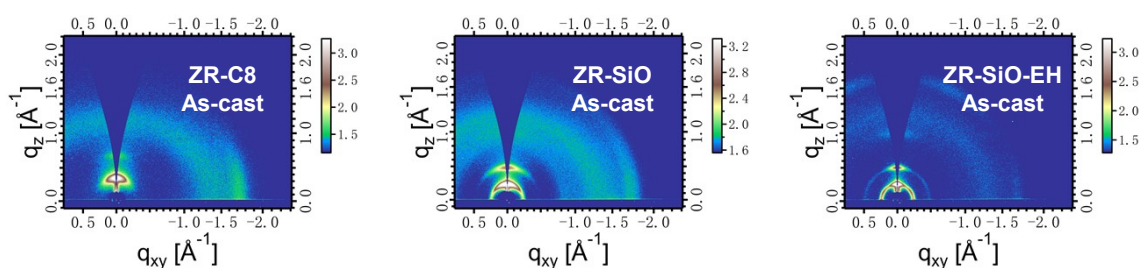
Figure S6 2D-GIWAXs patterns of ZR-C8, ZR-SiO, and ZR-SiO-EH as-cast films.
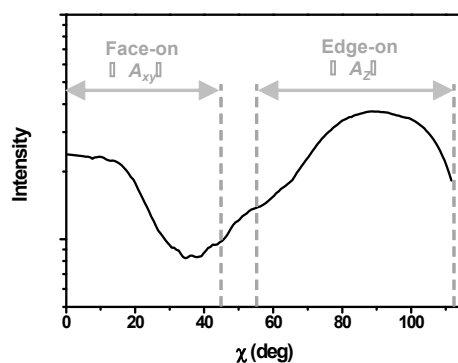
Figure S7 Pole figures extracted from the lamellar diffraction for ZR-SiO-EH pure film. Definitions of the polar angle (χ) range corresponding to the face-on (A_{xy}) and edge-on (A_z) crystallites are shown. The areas integrated with polar angle χ ranges of 0–45° (A_{xy}) and 55–115° (A_z) were defined as those corresponding to the fractions of face-on and edge-on crystallites, respectively.
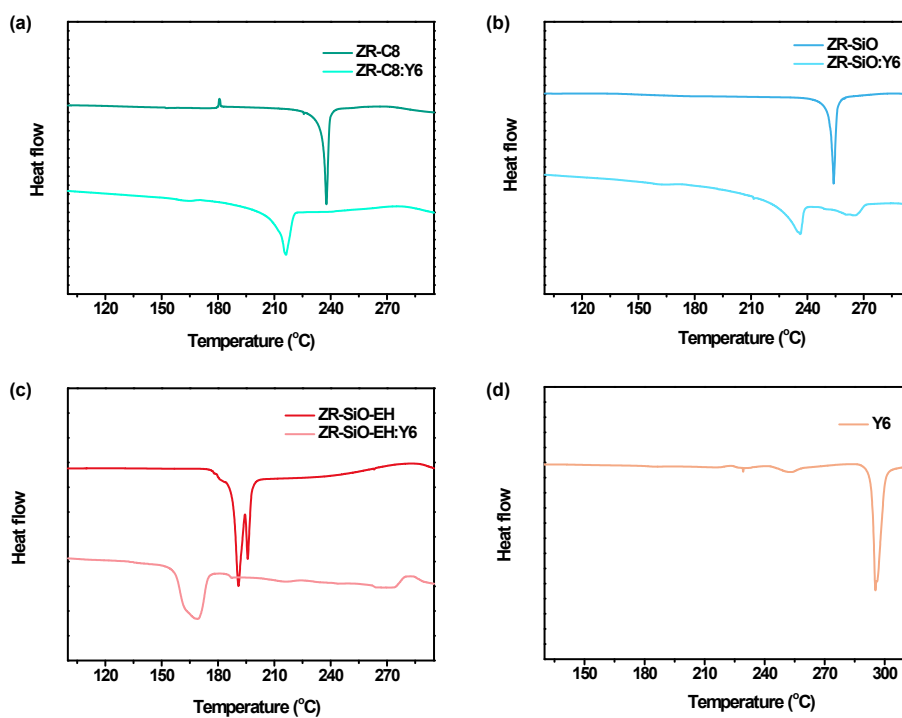
Figure S8 DSC thermograms of ZR-C8, ZR-SiO, ZR-SiO-EH, Y6, and their corresponding blends.
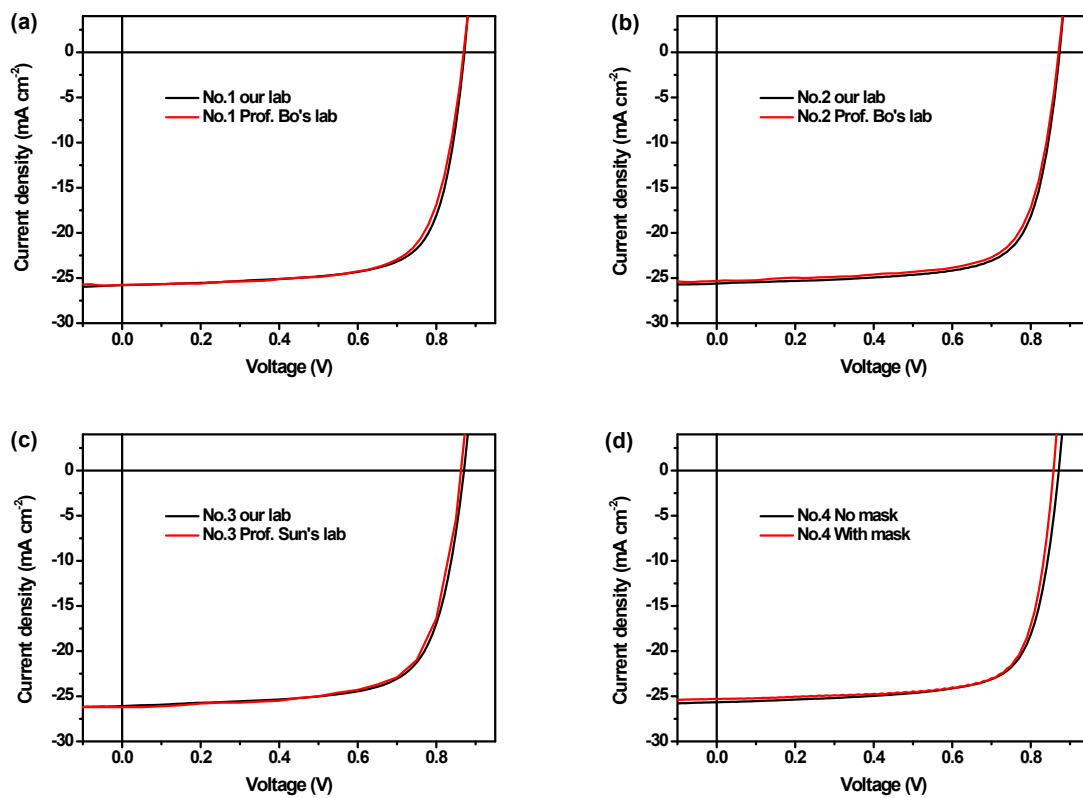
Figure S9 The *J-V* curves of four devices based on ZR-SiO-EH:Y6 -based device measured in our lab, Prof. Zhishan Bo's lab and Prof. Yanming Sun's lab and with mask.
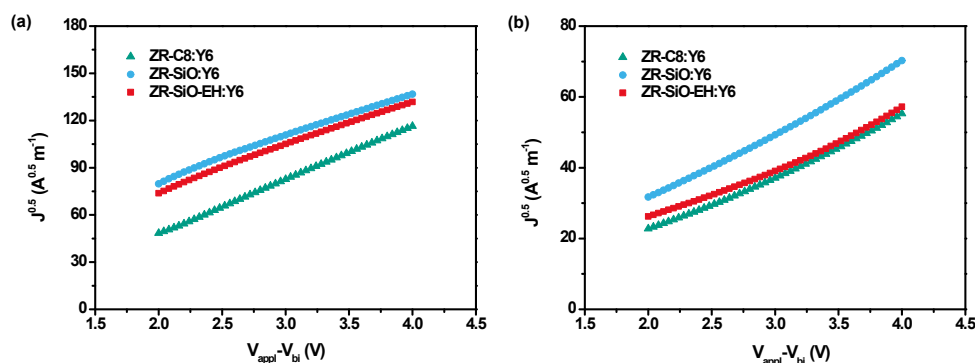
Figure S10 *J-V* characteristics along with the space-charge-limited current (SCLC) fitting of (a) hole-only and (b) electron-only devices for ZR-C8:Y6, ZR-SiO:Y6, and ZR-SiO-EH:Y6 blend films prepared under the optimal condition.
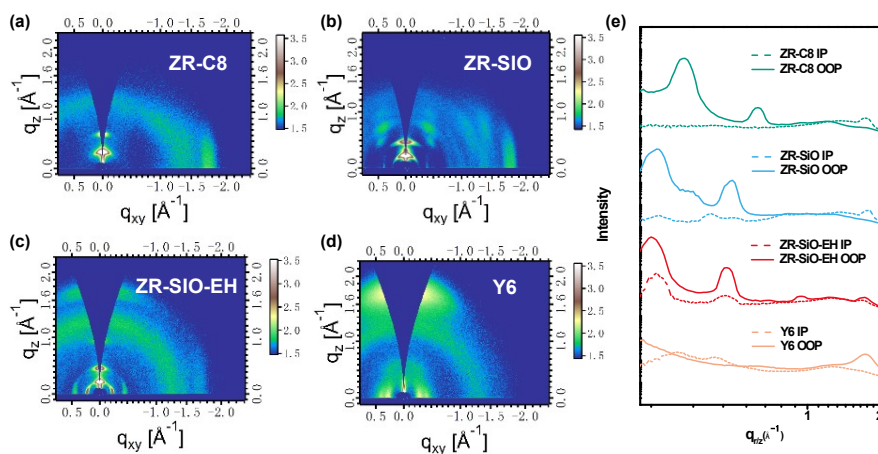
Figure S11 (a-d) 2-D GIWAXs patterns and (e) the corresponding line profiles of donors and acceptor with post treatment (120 °C-10min).
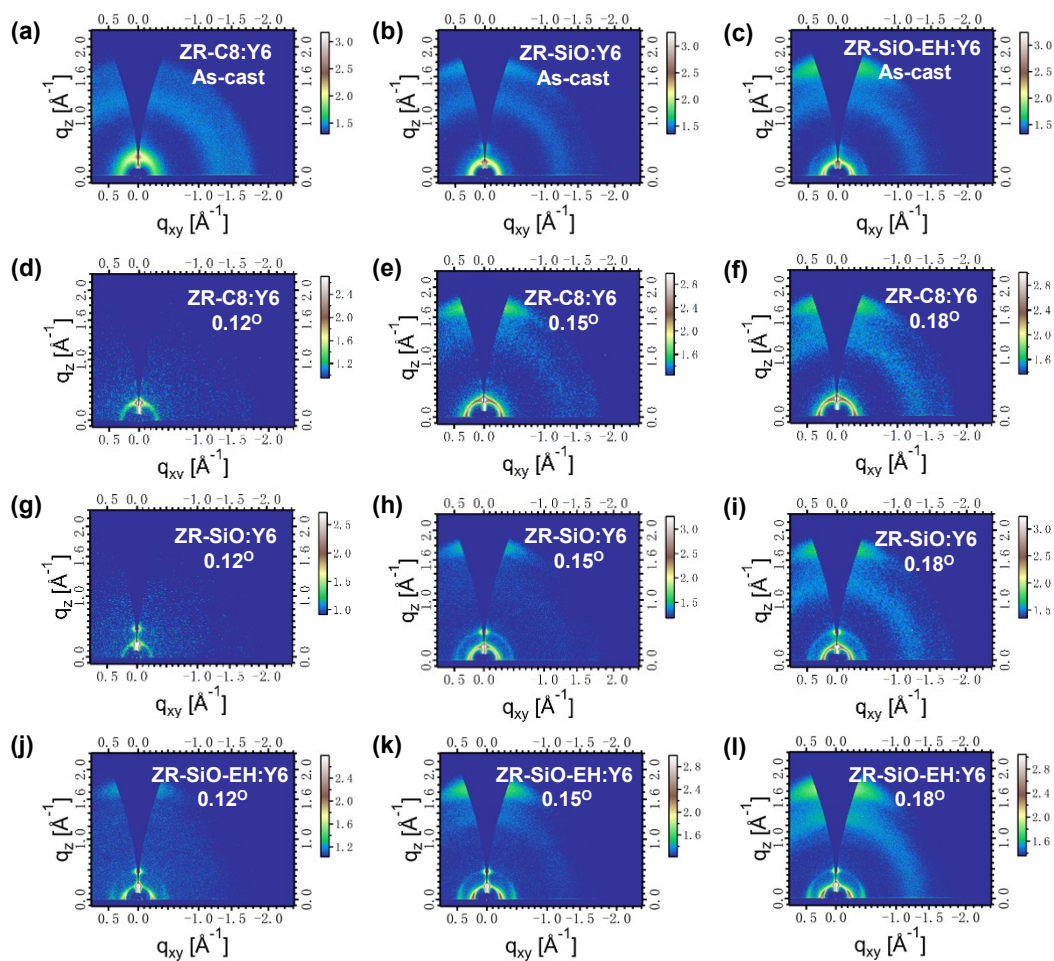
Figure S12 (a-c) 2-D GIWAXs patterns of ZR-C8:Y6. ZR-SiO:Y6 and ZR-SiO-EH:Y6 as-cast blend films; (d-l) 2-D GIWAXs patterns of optimal devices with different incidence angles.
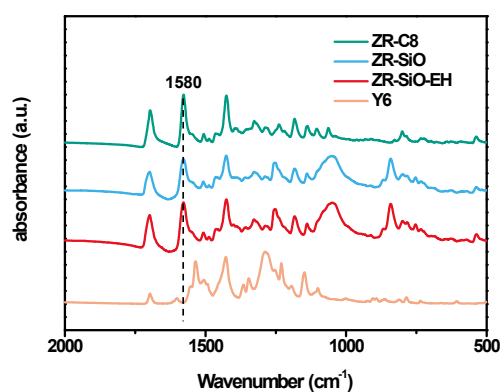
Figure S13 Infrared spectrogram of ZR-C8, ZR-SiO, ZR-SiO-EH and Y6.
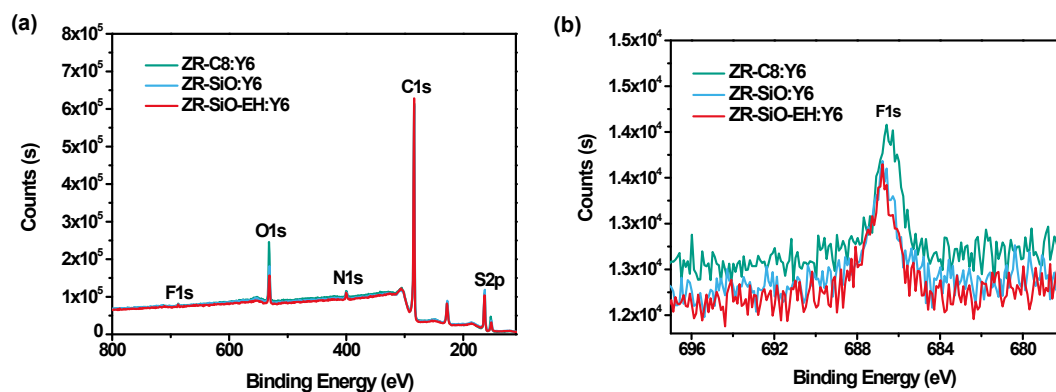
Figure S14 (a) XPS spectrum of optimal blend films; (b) F 1s XPS of optimal blend films revealed the presence of Y6 on the surface of the films.
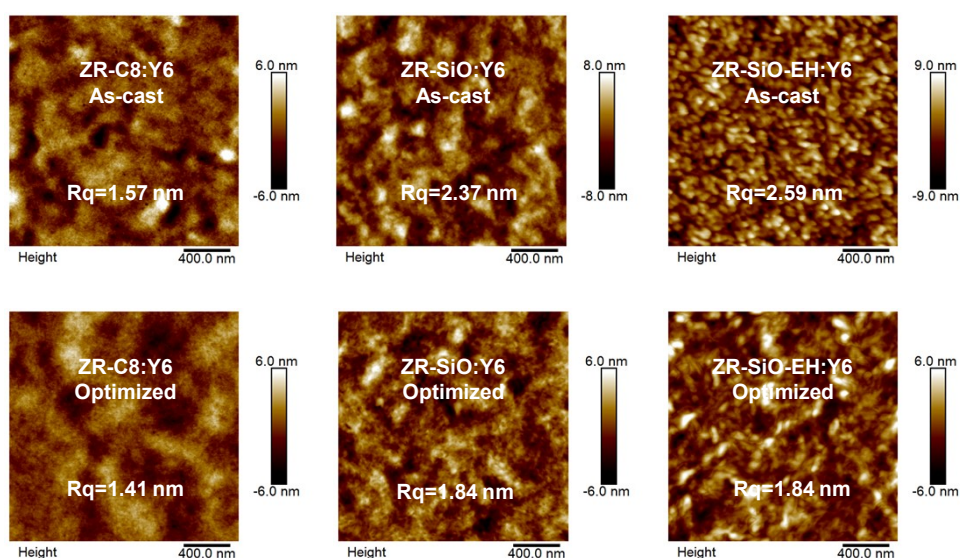
Figure S15 AFM images for three ASM systems (the surface roughness of the blend film for each system has been effectively decreased after optimization).
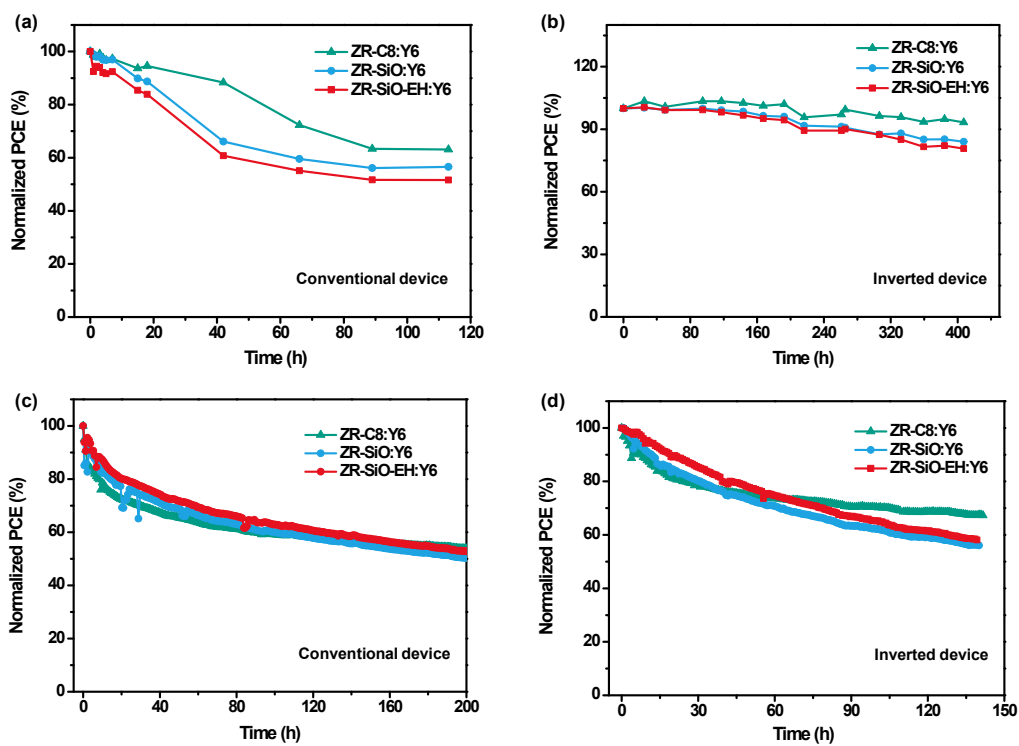
Figure S16 (a), (b) thermal stability (at 80 °C, N_2 atmosphere) and (c), (d) light stability

(N_2 atmosphere) of three ASM systems with conventional and inverted structures.

Supplementary Tables

Table S1 The comparison of high-performance binary ASM-OSCs (with PCE over 15%). Sort from low to high by PCE value.

System	V_{OC} (V)	J_{SC} (mA cm^{-2})	FF (%)	PCE (%)	Ref
BPF3T-C6:BO-4C	0.857	24.7	70.2	15.1	1
TBD-S4:Y6	0.854	24.53	72.1	15.1	2
B3T-P:BO-4Cl	0.815	25.7	72.4	15.2	3
B1:BO-4Cl	0.83	25.27	73	15.3	4
BTR-Cl:BTP-FCl-FCl	0.825	24.58	75.36	15.3	5
BT-2F:N3	0.845	24.28	75.02	15.39	6
SM-BF1:Y6	0.846	26.64	69.7	15.71	7
L2:Y6	0.83	26.35	72.1	15.8	8
M-PhS:BTP-eC9	0.84	25.4	75.6	16.2	9
ZR-SiO-EH:Y6	0.87	25.6	73.7	16.4	This work

Table S2 Optical and Electrochemical Properties of ZR-C8, ZR-SiO and ZR-SiO-EH.

Donor	λ_{max}^{sol}	λ_{max}^{film}	λ_{edge}^{film}	E_g^{opt}	E_{HOMO}	E_{LUMO}
ZR-C8	529.0	619.9	688.9	1.80	-5.30	-3.52
ZR-SiO	528.4	630.2	693.8	1.79	-5.38	-3.50
ZR-SiO-EH	532.3	617.3	681.4	1.82	-5.40	-3.48

Table S3 The HOMO energy levels of three small molecule donors, obtained by DFT, UPS and CV methods.

Donor	$E_{HOMO}{}^{Cal}$ [eV]	$E_{HOMO}{}^{UPS}$ [eV]	$E_{HOMO}{}^{CV}$ [eV]
ZR-C8	−5.029	−5.105	−5.30
ZR-SiO	−5.031	−5.165	−5.38
ZR-SiO-EH	−5.076	−5.214	−5.40

Table S4 Hole and electron mobilities of donors and optimal devices.

Films	μ_h (cm^2 V^{-1} s^{-1})	μ_e (cm^2 V^{-1} s^{-1})	μ_h/μ_e
ZR-C8	3.52×10^{-4}	-	-
ZR-SiO	4.46×10^{-4}	-	-
ZR-SiO-EH	6.92×10^{-4}	-	-
ZR-C8:Y6	3.98×10^{-4}	8.99×10^{-5}	4.43
ZR-SiO:Y6	2.58×10^{-4}	9.49×10^{-5}	2.73
ZR-SiO-EH:Y6	3.65×10^{-4}	1.03×10^{-4}	3.54

Table S5 Surface energy (γ) and Flory–Huggins interaction parameter (χ) obtained from water and diiodomethane contact angle measurement of different films.

films	θ_{H_2O} (deg)	$\theta_{CH_2I_2}$ (deg)	γ_d (mN m^{-1})	γ_p (mN m^{-1})	γ (mN m^{-1})	χ with Y6 (K)
ZR-C8	98.13	34.53	41.25	1.40	42.40	0.001
ZR-SiO	102.79	48.38	35.99	0.60	36.21	0.19
ZR-SiO-EH	102.59	52.22	33.31	1.08	34.64	0.32

Y6	92.14	38.94	37.38	4.05	41.60	-

Table S6 Calculation details of Flory–Huggins interaction parameter (χ) with DSC measurement data.

Substance 1	Substance 2	T_m (°C)	T_m^0 (°C)	ΔH_m (J/g)	$\varnothing_2$	χ
Y6	ZR-C8	215.99	237.69	27.52	0.667	0.11
Y6	ZR-SiO	236.13	253.94	27.75	0.667	0.75
Y6	ZR-SiO-EH	168.65	195.78	26.14	0.667	1.74

Table S7 Device optimization for ZR-C8:Y6 blends.

D/A	additive	Thermal annealing (°C)	V_{OC} (V)	J_{SC} (mA cm^{-2})	FF (%)	PCE (%)
1:0.5	—	—	0.849	11.36	28.86	2.78
1:0.5	—	120 (10min)	0.837	19.98	55.40	9.27
1:0.7	—	120 (10min)	0.834	20.94	52.01	9.08
1:0.4	0.2% CN	120 (10min)	0.831	24.43	57.96	11.77
1:0.5	0.2% CN	120 (10min)	0.829	25.01	58.82	12.20
1:0.5	0.3% CN	120 (10min)	0.820	25.31	55.76	11.58
1:0.5	0.5% CN	120 (10min)	0.834	24.51	54.47	11.13
1:0.6	0.2% CN	120 (10min)	0.829	24.73	54.89	11.26

Table S8 Device optimization for ZR-SiO:Y6 blends.

D/A	additive	Thermal annealing (°C)	V_{OC} (V)	J_{SC} (mA cm^{-2})	FF (%)	PCE (%)
1:0.5	—	—	0.874	19.99	48.08	8.40
1:0.5	—	120 (10min)	0.841	22.36	64.35	12.10
1:0.6	—	120 (10min)	0.836	21.48	57.08	10.25
1:0.7	—	120 (10min)	0.841	19.91	50.98	8.54
1:0.4	0.3% CN	120 (10min)	0.850	24.64	71.70	15.03
1:0.5	0.2% CN	120 (10min)	0.851	25.53	72.29	15.71
1:0.5	0.25% CN	120 (10min)	0.851	25.65	72.49	15.84
1:0.5	0.3% CN	120 (10min)	0.852	26.01	72.33	16.03
1:0.5	0.4% CN	120 (10min)	0.851	25.92	70.28	15.51
1:0.6	0.3% CN	120 (10min)	0.852	25.28	68.13	14.67

Table S9 Device optimization for ZR-SiO-EH:Y6 blends.

D/A	additive	Thermal annealing (°C)	V_{OC} (V)	J_{SC} (mA cm^{-2})	FF (%)	PCE (%)
1:0.5	—	—	0.890	20.38	60.58	10.99
1:0.6	—	—	0.871	18.23	58.63	9.31
1:0.5	—	100 (10min)	0.860	21.10	65.63	11.91
1:0.5	—	120 (10min)	0.843	21.57	66.13	12.01
1:0.5	—	140 (10min)	0.821	21.46	61.96	10.91
1:0.45	0.2% CN	120 (10min)	0.867	24.83	73.47	15.82
1:0.5	0.2% CN	120 (10min)	0.861	25.56	72.96	16.06

1:0.55	0.2% CN	120 (10min)	0.875	24.50	72.94	15.64
1:0.5	0.25% CN	120 (10min)	0.870	25.60	73.74	16.42
1:0.5	0.3% CN	120 (10min)	0.868	25.19	73.92	16.16
1:0.5	0.4% CN	120 (10min)	0.865	24.55	75.00	15.93
1:0.5	0.5% CN	120 (10min)	0.872	24.71	72.60	15.66

Table S10 Photovoltaic parameters of four devices based on ZR-SiO-EH:Y6-based device measured in our lab, Prof. Zhishan Bo's lab and Prof. Yanming Sun's lab and with mask (2.54 mm^2, Certificate No.: CDjc2022-00929).

Device Number	Condition	V_{OC} (V)	J_{SC} (mA cm^{-2})	FF (%)	PCE (%)
1	Our lab	0.871	25.80	72.98	16.40
	Prof. Bo's lab	0.869	25.83	72.07	16.18
2	Our lab	0.873	25.61	73.08	16.35
	Prof. Bo's lab	0.871	25.39	72.54	16.04
3	Our lab	0.870	26.10	71.33	16.20
	Prof. Sun's lab	0.863	26.17	70.90	16.01
4	No mask	0.871	25.66	73.38	16.40
	With mask	0.857	25.30	75.35	16.35

Table S11 The detailed date for exciton dissociation efficiency (η_{diss}) and charge collection efficiency (η_{coll}).

Devices	J_{ph}^{a}	J_{ph}^{b}	J_{sat}	η_{diss}	η_{coll}

	(mA cm^{-2})	(mA cm^{-2})	(mA cm^{-2})	(%)	(%)
ZR-C8:Y6	25.47	19.65	26.70	95.39	73.60
ZR-SiO:Y6	26.48	23.06	27.33	96.89	84.38
ZR-SiO-EH:Y6	25.22	22.52	25.84	97.63	87.15

[a] the photocurrent density was obtained under short-circuit condition.

[b] the photocurrent density was obtained under maximum power output condition.

Table S12 Relative element content of XPS test for ZR-C8:Y6, ZR-SiO:Y6 and ZR-SiO-EH:Y6 systems.

	ZR-C8:Y6	ZR-SiO:Y6	ZR-SiO-EH:Y6
Elements	Atomic (%)	Atomic (%)	Atomic (%)
C	77.74	76.70	79.29
F	0.48	0.55	0.61
N	2.55	2.47	2.07
O	10.60	6.89	5.93
S	8.62	8.58	8.10
Si		4.80	3.99

Table S13 The detailed date for R-SoXs.

	Relative domain purity	q (nm^{-1})	Domain size (nm)
ZR-C8:Y6	0.75	0.01	257.21
ZR-SiO:Y6	1	0.02	153.35
ZR-SiO-EH:Y6	0.81	0.03	112.06

Table S14 Detailed GIWAXs parameters of pristine and blend films with the grazing angle of 0.18°.

Film	(010) in in-plane			(010) in out-of-plane		
	Peak (Å^{-1})	d-spacing (Å)	CCL (Å)	Peak (Å^{-1})	d-spacing (Å)	CCL (Å)
ZR-C8	1.75	3.59	22.9	–	–	–
ZR-SiO	1.75	3.59	26.9	–	–	–
ZR-SiO-EH	1.70	3.70	19.6	1.74	3.61	21.4
Y6	–	–	–	1.75	3.59	20.5
ZR-C8:Y6	1.75	3.59	15.4	1.74	3.61	19.1
ZR-SiO:Y6	1.75	3.59	10.6	1.75	3.59	15.7
ZR-SiO-EH:Y6	–	–	–	1.75	3.59	23.3

D:\Data\2021new\202102\20210222\20210222-16 c8\0_B23\1

MALDI-TOF,CHCA,C8,20210222
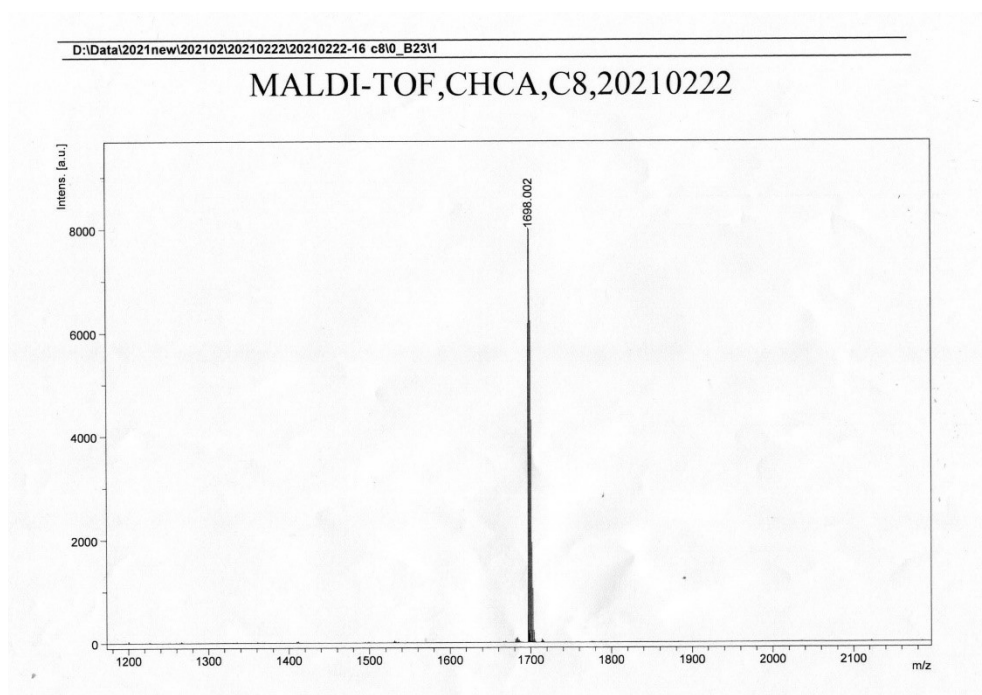
Figure S17 MALDI-TOF spectrum of ZR-C8.
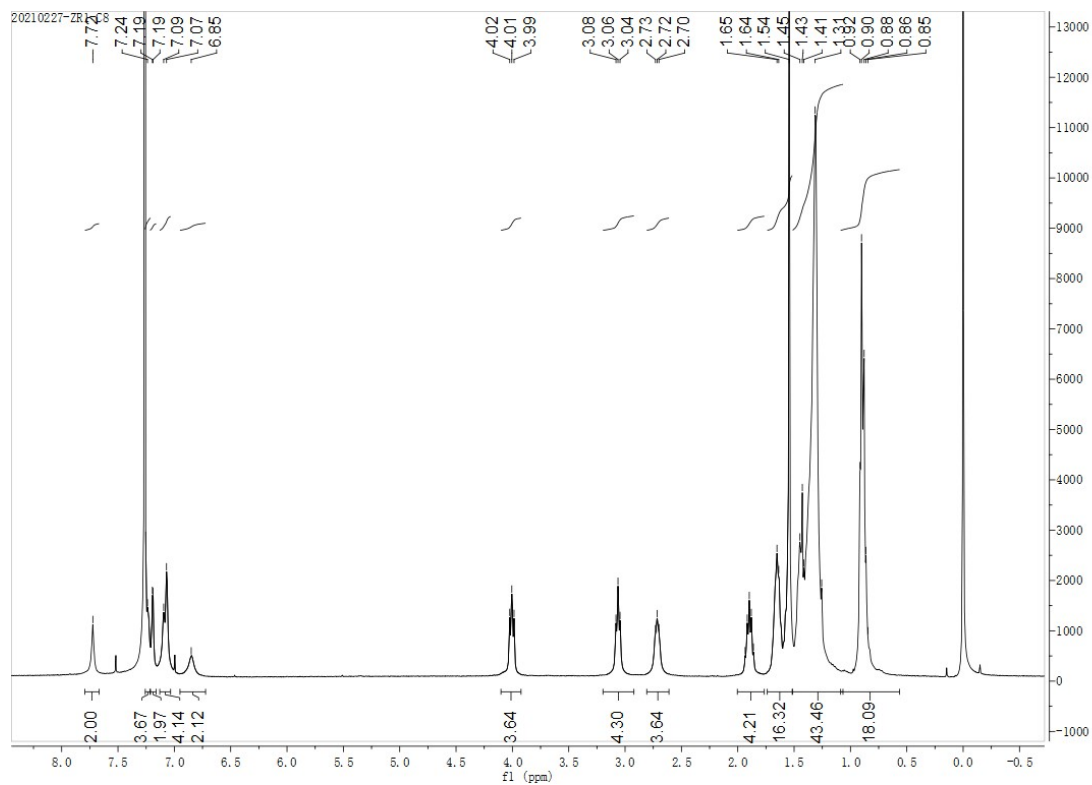
Figure S18 ^{1}H NMR spectrum of ZR-C8 in CDCl$_3$.
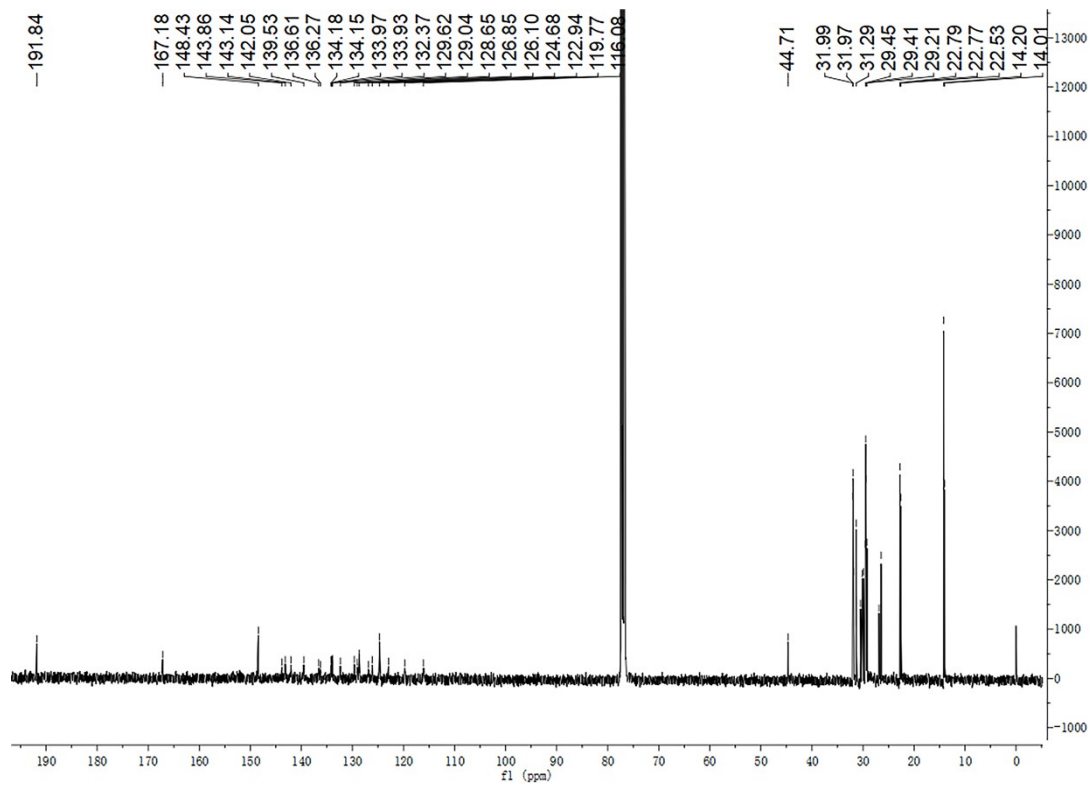
Figure S19 ^{13}C NMR spectrum of ZR-C8 in CDCl$_3$.

MALDI,SI,20210125.

Meas. m/z	#	Ion Formula	Score	m/z	err [ppm]	Mean err [ppm]	mSigma	rdb	e⁻ Conf	N-Rule
2080.540921	1	C100H140N2O6S14Si6	100.00	2080.541145	-0.1	0.2	56.5	38.0	odd	ok

Figure S20 MALDI-TOF spectrum of ZR-SiO.
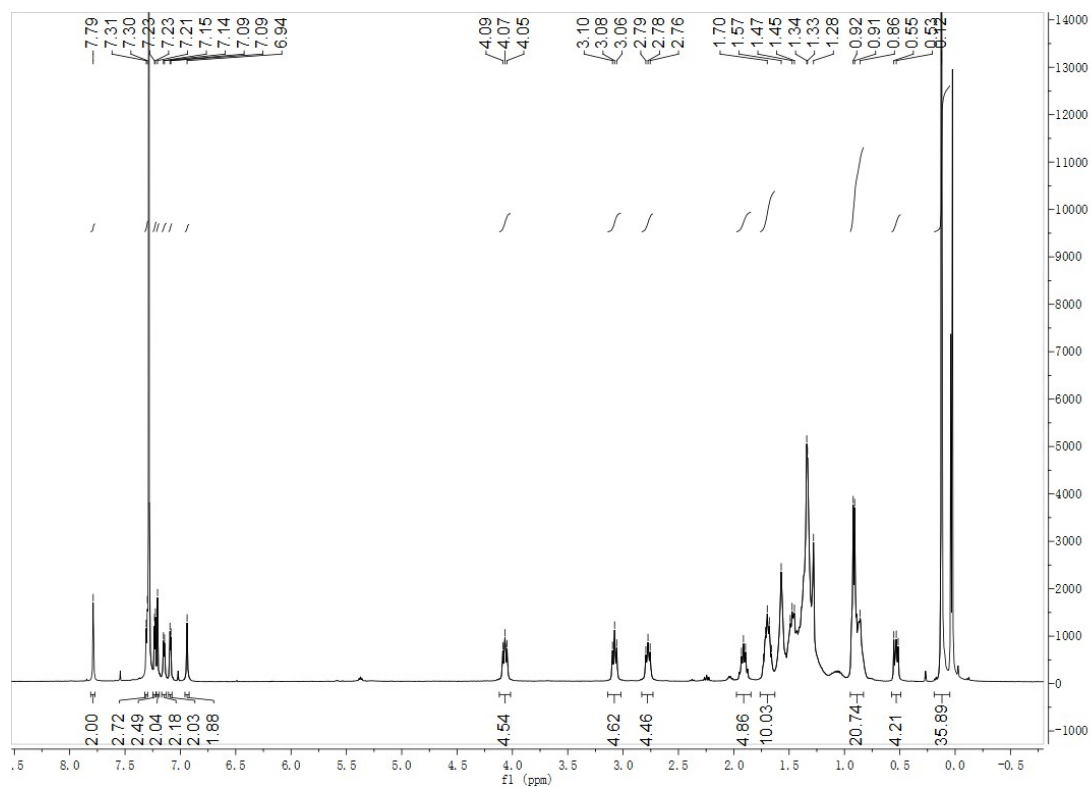
Figure S21 ^{1}H NMR spectrum of ZR-SiO in CDCl$_3$.
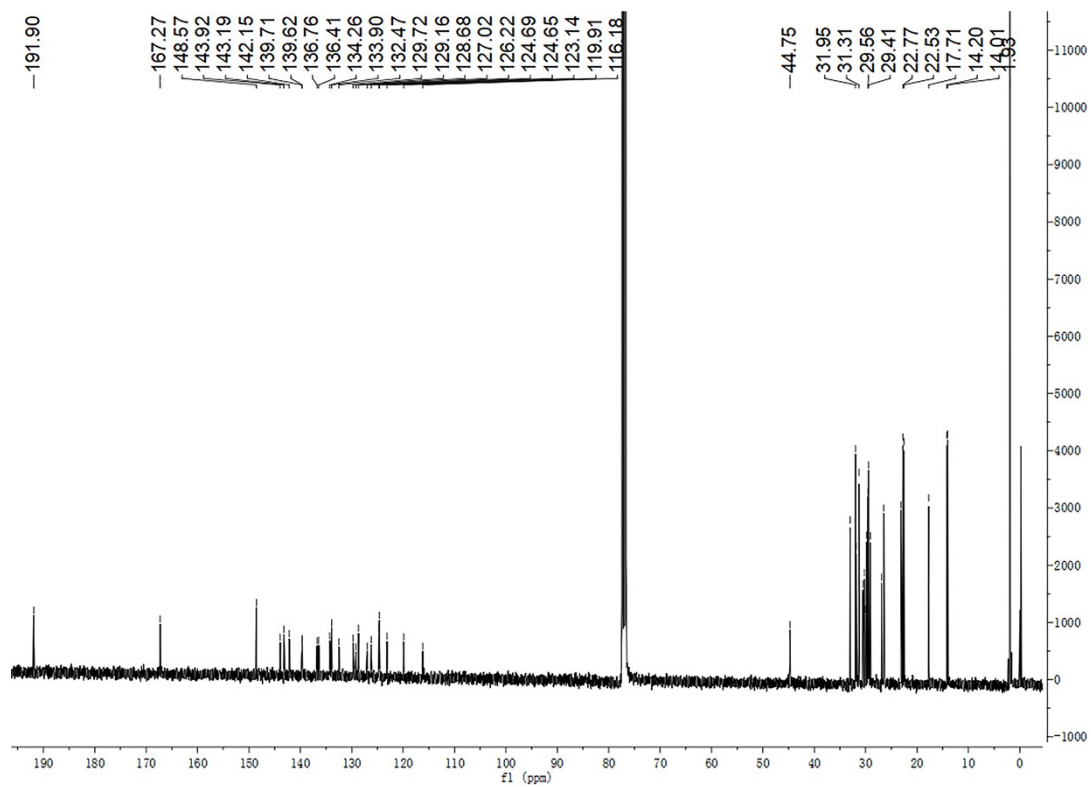
Figure S22 ^{13}C NMR spectrum of ZR-SiO in CDCl$_3$.

MALDI-TOF,chca,D24,20210525
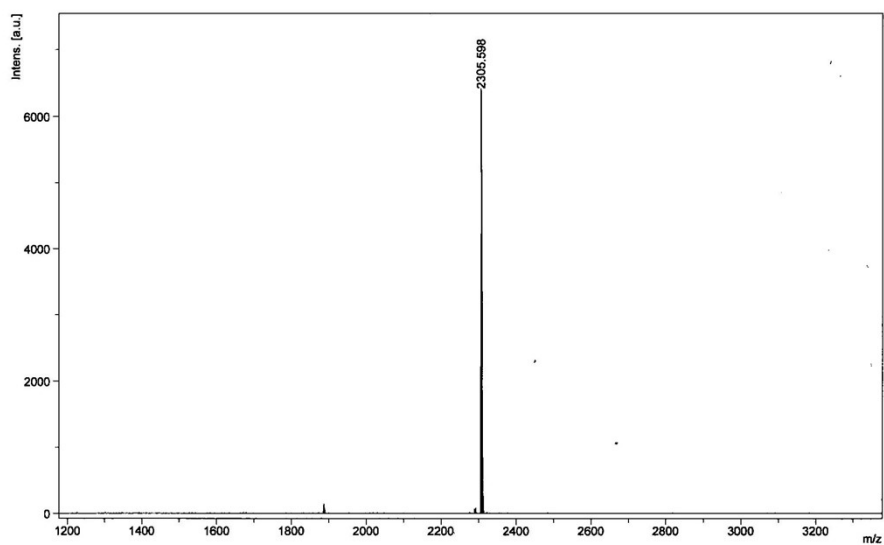
Figure S23 MALDI-TOF spectrum of ZR-SiO-EH.
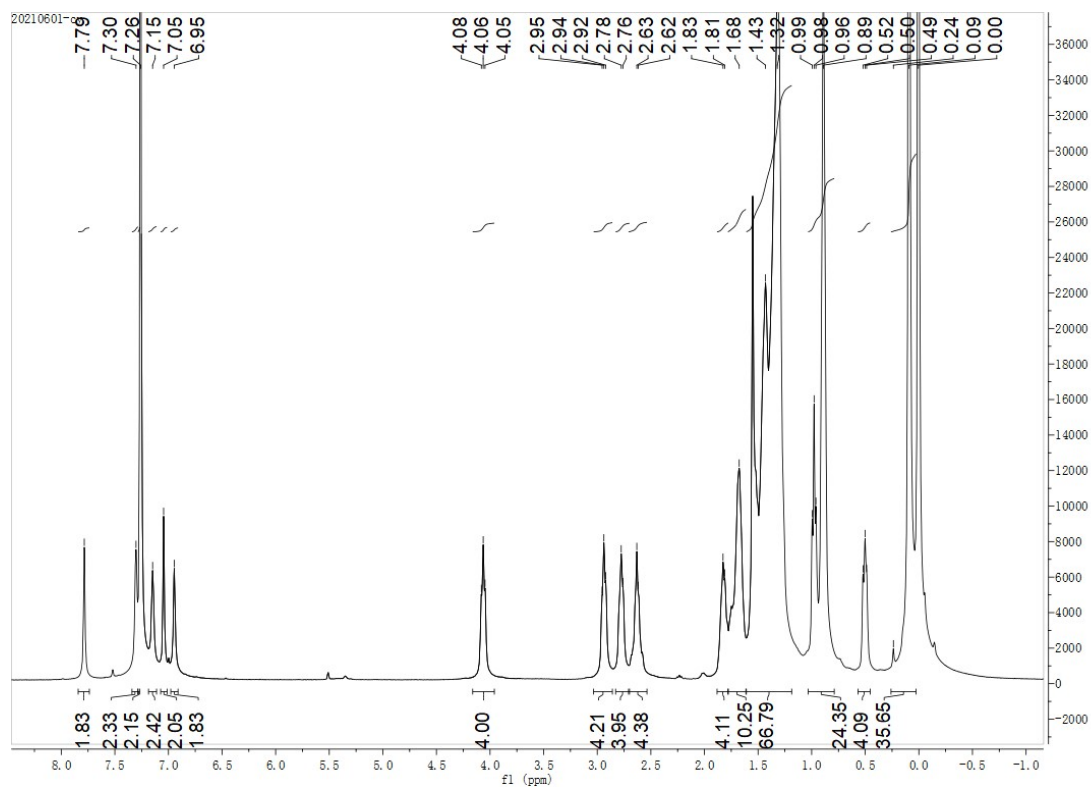
Figure S24 ^{1}H NMR spectrum of ZR-SiO-EH in CDCl$_3$.
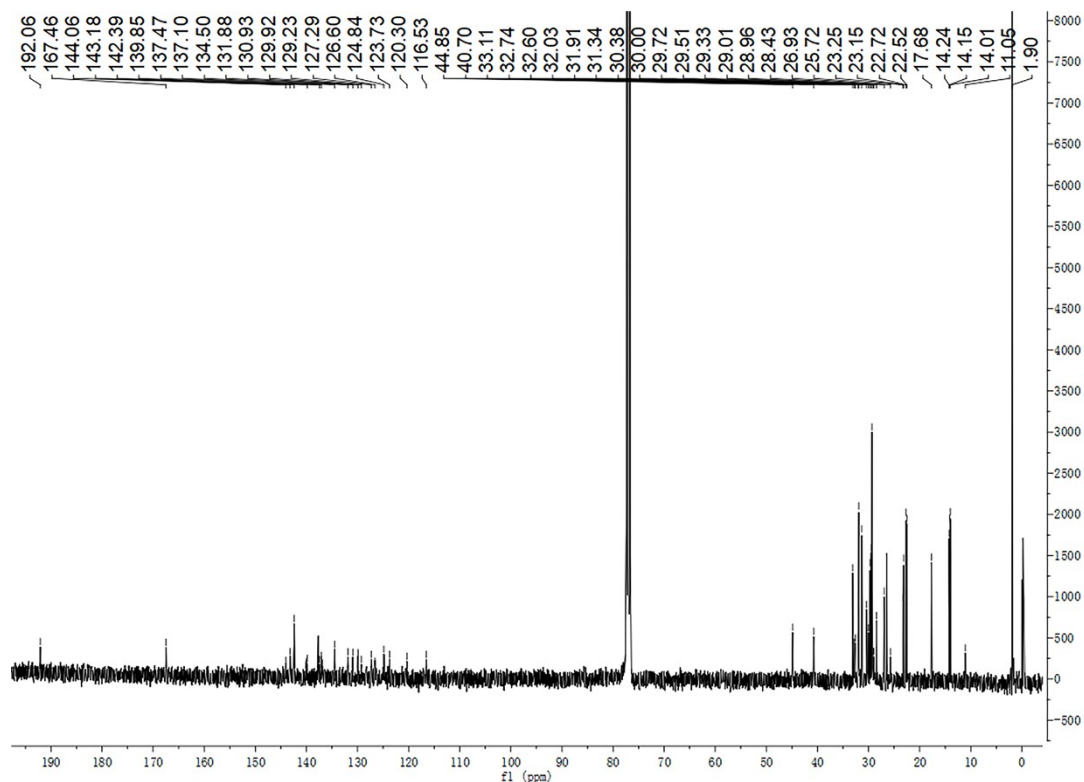
Figure S25 ^{13}C NMR spectrum of ZR-SiO-EH in CDCl₃.

Reference

1. Q. Lv, C. An, T. Zhang, J. Zhang, S. Zhang, P. Zhou, C. He and J. Hou, *Sci. China. Chem.*, 2021, **64**, 1200-1207.

2. X. Wang, J. Wang, J. Han, D. Huang, P. Wang, L. Zhou, C. Yang, X. Bao and R. Yang, *Nano Energy*, 2021, **81**, 105612.

3. C. An, Y. Qin, T. Zhang, Q. Lv, J. Qin, S. Zhang, C. He, H. Ade and J. Hou, *J. Mater. Chem. A*, 2021, **9**, 13653-13660.

4. J. Qin, C. An, J. Zhang, K. Ma, Y. Yang, T. Zhang, S. Li, K. Xian, Y. Cui, Y. Tang, W. Ma, H. Yao, S. Zhang, B. Xu, C. He and J. Hou, *Sci. China. Mater.*, 2020, **63**, 1142.

5. D. Hu, Q. Yang, Y. Zheng, H. Tang, S. Chung, R. Singh, J. Lv, J. Fu, Z. Kan, B. Qin, Q. Chen, Z. Liao, H. Chen, Z. Xiao, K. Sun and S. Lu, *Adv. Sci.*, 2021, **8**, 2004262.

6. J. Ge, L. Hong, W. Song, L. Xie, J. Zhang, Z. Chen, K. Yu, R. Peng, X. Zhang and

Z. Ge, *Adv. Energy Mater.*, 2021, **11**, 2100800.

7. J. Guo, B. Qiu, D. Yang, C. Zhu, L. Zhou, C. Su, U.-S. Jeng, X. Xia, X. Lu, L. Meng, Z. Zhang and Y. Li, *Adv. Funct. Mater.*, 2022, 2110159.

8. T. Xu, J. Lv, K. Yang, Y. He, Q. Yang, H. Chen, Q. Chen, Z. Liao, Z. Kan, T. Duan, K. Sun, J. Ouyang and S. Lu, *Energy Environ. Sci.*, 2021, **14**, 5366-5376.

9. L. Zhang, X. Zhu, D. Deng, Z. Wang, Z. Zhang, Y. Li, J. Zhang, K. Lv, L. Liu, X. Zhang, H. Zhou, H. Ade and Z. Wei, *Adv. Mater.*, 2022, **34**, 2106316.